This is the peer reviewed version of the following article:

Alberdi, B., Oyanguren, A., Ulacia, I. and Larrañaga, J. (2025), Effect of Roll Forming Process Imperfections on the Buckling Capacity of Racked Beams. ce/papers, 8: 330-336.

which has been published in final form at

https://doi.org/10.1002/cepa.70067

Full paper

Effect of Roll Forming Process Imperfections on the Buckling Capacity of Racked Beams

Beñat Alberdi[1] | Aitor Oyanguren[1] | Ibai Ulacia[1] | Jon Larrañaga[1]

Correspondence

Mr. Beñat Alberdi
Mondragon University
Faculty of Engineering
Loramendi 4
20500 Mondragon
Email: benat.alberdio@alumni.mondragon.edu

[1] Mondragon Unibertsitatea, Faculty of Engineering, Mechanical and Industrial Production Department, Arrasate-Mondragon, Spain

Abstract

Ensuring the stability and safety of steel storage racks is essential to withstand applied loads over time. Rack columns are typically produced through a cold roll-forming, enabling high productivity and open-section profiles, known as uprights. However, roll-forming imperfections can adversely affect buckling capacity. Stub column compression tests, as defined by the EN 15512 standard, experimentally determine the buckling capacity, while numerical methods further analyze it. A common way to introduce geometric imperfections in FEM models is by superposing scaled eigenmodes obtained from an elastic buckling analysis. Although standards specify imperfection types (local, distortional, global) and magnitudes, combining them remains unclear, often requiring multiple scenarios that may overly penalize capacity, as some imperfections rarely occur simultaneously.

This work determines imperfection values from predefined roll-forming imperfections and identifies which combination most significantly affects open-section column buckling capacity. The initial roll-forming imperfections were measured and each amplitude established. A FEM model incorporating these imperfections was developed and validated against experimental data. Finally, the effects of these errors and their most critical combination on buckling capacity were determined, contributing to improved design procedures and a more reliable assessment of structural performance.

Keywords

Steel storage racks, Manufacturing imperfections, Buckling, Numerical analysis.

1 Introduction

Thin-walled structures play a crucial role in modern structural engineering, particularly in applications where weight and strength optimization are essential, such as industrial shelving systems. However, these structures present specific challenges due to their susceptibility to buckling phenomena.

In most cases of shelving system uprights, geometric imperfections resulting from the roll-forming process critically affect the buckling capacity. These imperfections are related to the manufacturing process and therefore exhibit specific patterns that can be characterized and modelled. However, their impact on structural stability depends on their magnitude, distribution and interaction, which complicates both the structural analysis and the design of the uprights.

Minimizing imperfections is a common challenge in the roll forming process, where steel sheets are incrementally shaped by means of cold bending to achieve precise geometries. These defects are caused by the accumulation of secondary deformations that occur throughout production. Factors such as residual stresses, misalignments in machinery or variations in material properties can cause deviations that compromise the structural integrity and performance of the final profiles.

The geometric imperfections have been defined by several authors, including Halmos [1]. Six of the most common geometric imperfections generated during roll-forming are included in the study. Longitudinal bow, which is a vertical curvature along the length of the profile. Camber, which is a lateral deviation perpendicular to the rolling direction. Twist, which involves a rotation of the cross-section along the longitudinal axis. Springback, which results from elastic recovery after forming and causes dimensional deviations. Cross bow, which is a transverse curvature across the web of the section. Flare, which is characterized by variations in the flange angle along the profile where the flange flares outward or inward relative to the web. Moneke & Groche [2] described two types of flaring depending on the residual stresses. The first type is caused by the torsional moment generated from residual shear stresses, where the lead end flares in, and the tail end flares out. In the second type, both profile ends flare out due to a bending moment generated by longitudinal residual stresses. In practice, both mechanisms coexist, and the visible flare at each end of the section results from the combined release of torsional and bending moments. Other imperfections such as waving are not considered in this study.

Several studies have addressed the influence of geometric imperfections in the buckling capacity of thin-walled structures. The most common approach to introducing these imperfections into FEM models is by incorporating the displacements obtained from lineal buckling mode analyses. Among other studies, Bonada et al. developed various models to estimate the initial imperfections that should be considered in FEM analyses [3]. Sena Cardoso & Rasmussen took a different approach by defining geometric imperfections directly linked to the roll-forming process and integrating them into FEM simulations [4]. Additionally, Bonada et al. investigated the effects of cold work on structural performance by simulating the roll-forming process itself [5].

More recently, innovative methods have emerged for capturing initial geometric imperfections with higher precision. Xu et al. [6] developed a technique that employs laser scanning combined with advanced data processing to generate accurate models of initial geometric imperfections, closely predicting the initial geometry of steel members.

Until now, initial imperfections have not been directly related to manufacturing process imperfections, which allows for a better understanding of the initial condition of the uprights. In this study, a new methodology has been developed to measure, define, and implement geometric imperfections resulting from the roll-forming process. The approach is based on measurements obtained using a Coordinate Measurement Machine (CMM). The aim of the study is to validate a model which includes the geometric imperfections resulting from roll-forming process and evaluate the influence of them in order to identify those with the greatest impact on the buckling capacity of the upright.

2 Definition of the geometric imperfections

Roll forming imperfections considered in this study are shown in Figure 1 and are classified into two types: global and local defects. Global defects, such as longitudinal bow, camber and twist, impact the entire length of the profile, resulting in deviations in straightness or angular distortion. On the other hand, local defects, including flare, cross bow and springback are limited to specific regions of the profile, causing localized irregularities.

2.1 Longitudinal bow (LB) and camber (C)

Regarding longitudinal bow and camber, these have been modelled using a parabolic function along the upright, which corresponds to a second-degree polynomial. The amplitude of the imperfection corresponds to the maximum value of the parabola.

$$\delta_{LB}(z) = -\frac{4 \cdot A_{LB}}{L^2} \cdot z^2 + \frac{4 \cdot A_{LB}}{L} \cdot z \tag{1}$$

$$\delta_{C}(z) = -\frac{4 \cdot A_{C}}{L^2} \cdot z^2 + \frac{4 \cdot A_{C}}{L} \cdot z \tag{2}$$

A_{LB} and A_C are the amplitude of the imperfection at the maximum point, while L is the length of the profile, z the longitudinal direction and δ_{LB} and δ_C the imperfection value at each point of the profile.

2.2 Twist (T)

In the case of twist, its trend along the uprights is linear, with a continuous rotation. Therefore, it has been represented using a first-degree polynomial, i.e., a straight line.

$$\theta_T(z) = \frac{A_T}{L} \cdot z \tag{3}$$

Where the amplitude (A_T) and the imperfection value at each length (θ_T) are given in degrees (º).

2.3 Flare (F)

The midpoint of the profile (z = L/2) is considered the neutral axis, where the combined flare effect is zero. Therefore, it is modelled using a parabolic function along the longitudinal direction.

$$\theta_F(z) = \frac{2(A_{F1} + A_{F2})}{L^2} \cdot z^2 - \frac{3(A_{F1} + A_{F2})}{L} \cdot z + A_{F1} \tag{4}$$

A_{F1} is the amplitude of the flare at one end of the profile, while A_{F2} is the amplitude at the other end. In this case, A_{F1}, A_{F2} and θ_F are also expressed in degrees (º).

Due to possible combinations of the two flare types, in this work, type 1 flare (FT1) refers to the case where the lead end flares in and the tail end flares out (predominantly influenced by shear stresses), while type 2 flare (FT2) refers to the case where both profile ends flare out (mainly influenced by longitudinal bending stresses). Thus, if one of the amplitudes is positive and the other negative, the flare is classified as type 1. If both amplitudes are positive, it is classified as type 2.

2.4 Springback (SB)

The springback imperfection value, which is also the angle of the flanges, is constant along the profile, as the differences in the angle of the flanges are considered as flare.

$$\theta_{SB}(z) = A_{SB} \tag{5}$$

2.5 Cross bow (CB)

For cross bow, it has also been defined by a parabolic function, but in this case, it describes variations across the web of the profile rather than along the upright, where w is the length of the web and x the transversal direction of the profile. This parabola remains constant throughout the length of the upright.

$$\delta_{CB}(x) = A_{CB} \cdot \left(1 - \frac{x^2}{\left(\frac{w}{2}\right)^2}\right) \tag{6}$$

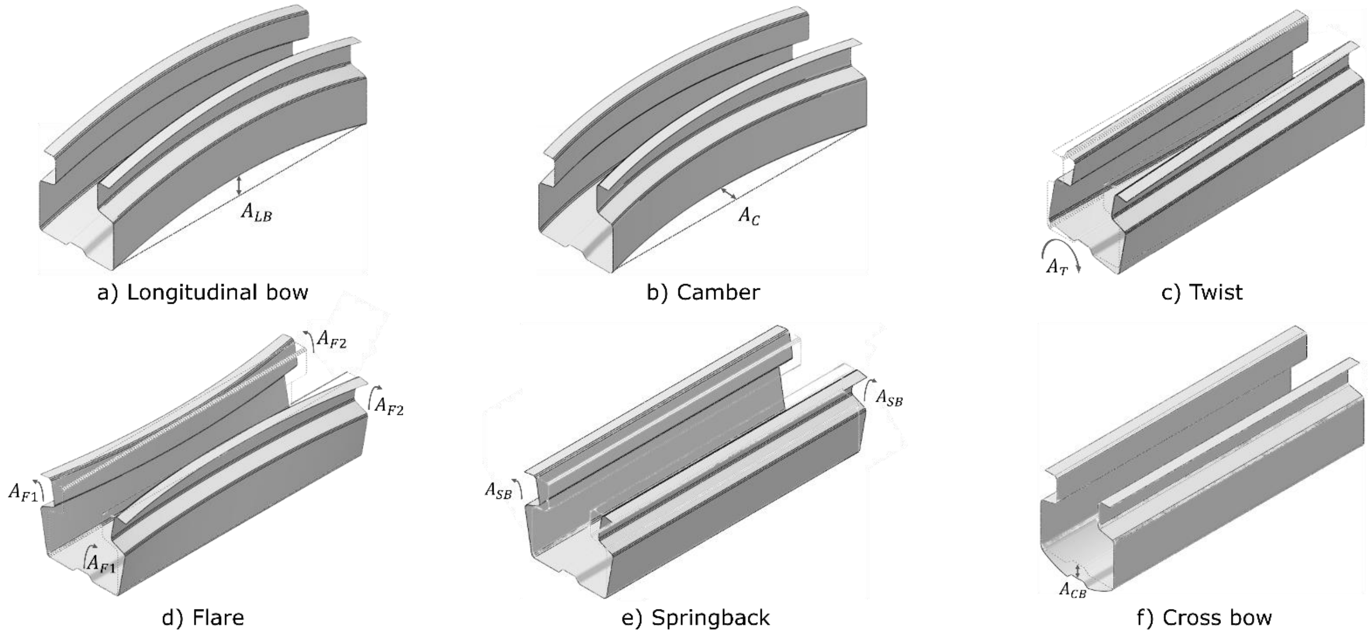

Figure 1 Geometric imperfections resulting from roll-forming process.

3 Numerical model

To accurately capture the effects of the geometric imperfections and evaluate them, a nonlinear finite element model was developed. A custom computational tool is used to automate the setup of the models, where the previously measured and parameterized imperfections are incorporated into the model. A 3D mesh is generated using linear quadrilateral shell elements of type S4R and imported into Abaqus, with an average element size of 2 mm.

The stress-strain behaviour of the material is modelled using a bilinear isotropic hardening approach to replicate the elastoplastic behaviour of cold-formed steel. This includes an elastic region followed by a plastic region where hardening follows a linear relationship.

The numerical model, shown in Figure 2, incorporates pinned supports at both ends of the upright to replicate the experimental boundary conditions under compressive loads. To achieve this, two reference points (RPs) are defined, one at each end of the upright. The first RP represents the free end, where the compressive force is applied. At this point, the only allowed translation is axial translation, while torsional rotation is constrained (U1=U2=UR3=0). The second RP stabilizes the upright by simulating the pinned support behaviour, constraining translations along all three axes and torsional rotation (U1=U2=U3=UR3=0). A coupling constraint connects each RP to its respective contact surface on the upright, ensuring that forces and displacements are distributed uniformly across the cross-section. These RPs are located at a distance corresponding to the radius of the ball bearing and the thickness of the plates used in the experimental setup, as specified by the European standard EN 15512:2020 [7], simulating its behaviour. In this case they are located at 55 *mm* from the profile ends, at the height of the centre of gravity of the net profile.

The analysis uses the Riks method to capture the buckling and post-buckling behaviours under axial compression, employing a single step. This method, also known as the arc-length method, allows tracing the equilibrium path beyond limit points by controlling both the load and displacement increments, making it suitable for instability problems.

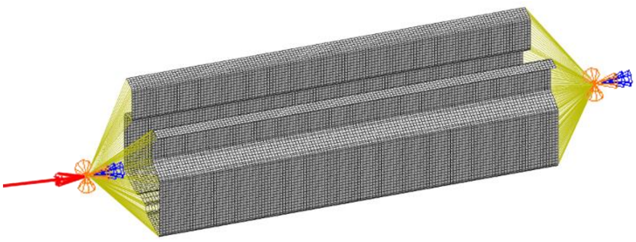

Figure 2 Shell meshed numerical model.

4 Experimental procedure

4.1 Profile measurement

The raw profiles were measured using a Coordinate Measuring Machine (CMM) as shown in Figure 4. The coordinates of several points along the profile section were recorded each 25 mm, with the profile length determining the number of measured sections. These measured points are processed through a custom-developed program designed to analyse and interpret the data accurately.

This data processing provides two optional outputs. On one hand, a mesh can be generated from the measured points, where the number of nodes can be customized both within each section and along the length of the profile. On the other hand, the imperfections can be quantified by calculating the deviations from the ideal profile, providing a detailed assessment of the previously defined geometric imperfections. The steps of each process are shown in Figure 3.

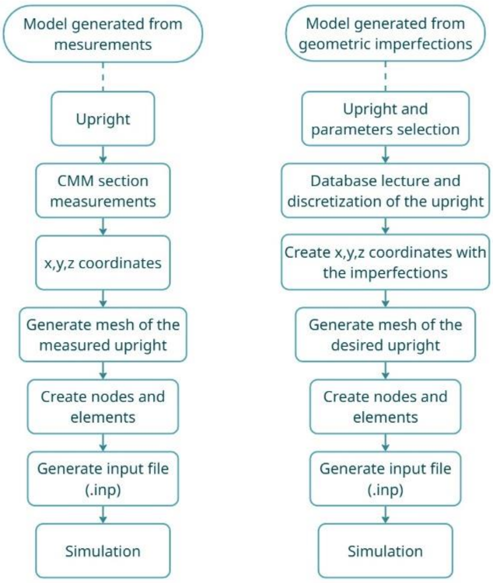

Figure 3 Flowchart of the presented methodology.

4.2 Buckling experiments

The experimental tests to determine the buckling resistance of the upright were conducted according to the compression tests on uprights described in the European standard EN 15512:2020 [7], as shown in Figure 4.

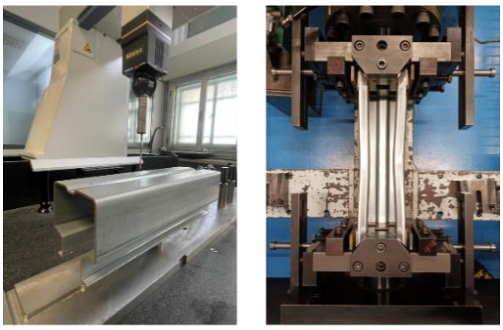

a) b)

Figure 4 Experimental procedures. a) CMM measurements b) Compression test of the upright.

5 Geometry and case studies

In this study, two uprights without perforations were used, each having the same geometry (Figure 5) but different dimensions. The nominal dimensions were used, and for each upright, different lengths were examined. Figure 5 summarizes the uprights employed in the study, where w_u, f_u and t_u represent the web, flange and thickness of the upright, respectively.

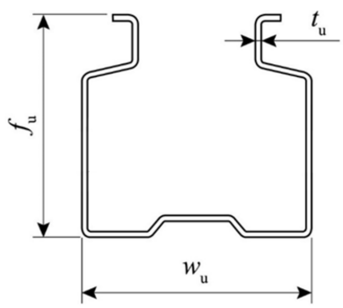

Upright	U80	U120
Web [w_u]	80	120
Flange [f_u]	65.55	114
Thickness [t_u]	1.8	3
Lengths	350 - 2000	400 - 2000

Figure 5 Cross sections parameters of the analysed uprights.

Initially, four uprights of each profile type were measured: the U80 uprights with a length of 350 mm, and the U120 uprights with a length of 400 mm. From these measurements, and after appropriate data processing, the amplitudes of the defined geometric imperfections were determined. These amplitudes were calculated based on the average imperfections observed across the measured profiles.

The next step involved the validation of the numerical models through simulations. Experimental results were compared with models generated both directly from the measured profiles and from idealized imperfections characterized by their corresponding amplitudes. Specifically, two types of models were developed: models reproducing the exact measurements of each profile and models incorporating geometric imperfections based on the defined amplitudes for each case. Additionally, both the thickness of each upright and the real material properties (obtained through tensile testing) were also considered.

Finally, an analysis was conducted to evaluate the effect of geometric imperfections on the buckling capacity of the uprights. Initially, each imperfection was assessed individually for different lengths. Both types of flare were analysed. Subsequently, combined imperfections were studied by considering all possible combinations, always including the imperfection that had the most significant individual influence.

6 Results and discussion

6.1 Geometric imperfection amplitudes

From the measurements obtained from the uprights, the amplitudes of the geometric imperfections for each type of imperfection and each upright type were determined, as presented in Table 1.

Table 1 Average amplitudes of the measured uprights.

Imperfection		Amplitude U80	Amplitude U120	Unit
Global	Longitudinal bow (A_{LB})	0.19 (L/1842)	0.92 (L/435)	mm
	Camber (A_C)	0.07 (L/5000)	0.03 (L/13333)	mm
	Twist (A_T)	0.36 (L/972)	0.09 (L/4444)	o
Local	Springback (A_{SB})	0.58 (f/113)	0.24 (f/475)	o
	Flare 1 (A_{F1})	2.40 (f/27.3)	0.42 (f/271)	o
	Flare 2 (A_{F2})	0.17 (f/385)	-0.38 (f/300)	o
	Cross bow (A_{CB})	1.24 (0.69t)	0.78 (0.26t)	mm

However, due to the limited number of samples, which restricted the accurate definition of the imperfection amplitudes for each upright, the subsequent analyses of individual and combined imperfections were based on the imperfection amplitudes recommended by Pastor et al.

[8] and by EN 1993-1-5:2006/AC:2009 [9] for initial imperfections depending on the buckling mode considered. Moreover, with the amplitudes shown in Table X, most imperfections are either amplified or take values close to the maximum measured. In particular, the amplitudes associated with springback and flare were taken as representative of distortional modes, given that these imperfections primarily affect the flange, while for cross bow were considered the amplitudes of local modes. In the case of the flare, the same value has been assigned to both extremes, whether positive or negative.

Table 2 Amplitudes of the imperfections employed in the analysis.

Imperfection		Amplitude	Unit
Global	Longitudinal bow	L/500	mm
	Camber	L/1000	mm
	Twist	L/1000	º
Local	Springback	f/50	º
	Flare	f/50	º
	Cross bow	0.34t	mm

6.2 Validation of the model

For the validation of the model, both the one generated from the measured coordinates and the one generated from the geometric imperfections were compared with the results obtained from the experimental tests. Table 3 shows the average maximum load of the 4 cases for each type of test, with the standard deviation and the relative error of the FEM models.

Table 3 Results and comparison of the tests.

Model	Type of test	Rk [kN]	σ	Error [%]
U80	Experimental	157.02	1.97	-
	FEM measured coordinates	144.98	3.18	7.67
	FEM geometric imperfections	144.81	4.05	7.78
U120	Experimental	444.63	3.23	-
	FEM measured coordinates	417.54	1.03	6.09
	FEM geometric imperfections	419.48	1.21	5.66

By evaluating the discrepancies between predicted and observed responses, the validity of the modelling approach can be established, ensuring that the numerical representation accurately captures the effects of geometric imperfections.

6.3 Analysis of the imperfections

First, the geometric imperfections were analysed individually for each upright. The reduction in buckling capacity caused by each imperfection is relative to the perfect model for each length, as shown in Figure 6. The load application point was kept unchanged at the centre of gravity of the perfect profile. The results indicate that the influence of imperfections varies significantly with changes in upright length. In most cases except with some local imperfections, the reduction in buckling capacity increases as the length of the upright increases.

For global imperfections (Figure 6a), this trend is expected, as longer uprights have larger initial geometric imperfections and lower overall stability. These global imperfections considerably reduce the buckling resistance of the upright, with reductions exceeding 15% for the longest specimens for U120 profile and up to 50% for U80. Local imperfections (Figure 6b) have a lesser impact on the buckling resistance compared to global imperfections in the case of the U120 profile, except for flare imperfections in short specimens. However, for the U80 profile, local imperfections have an impact comparable to that of global imperfections.

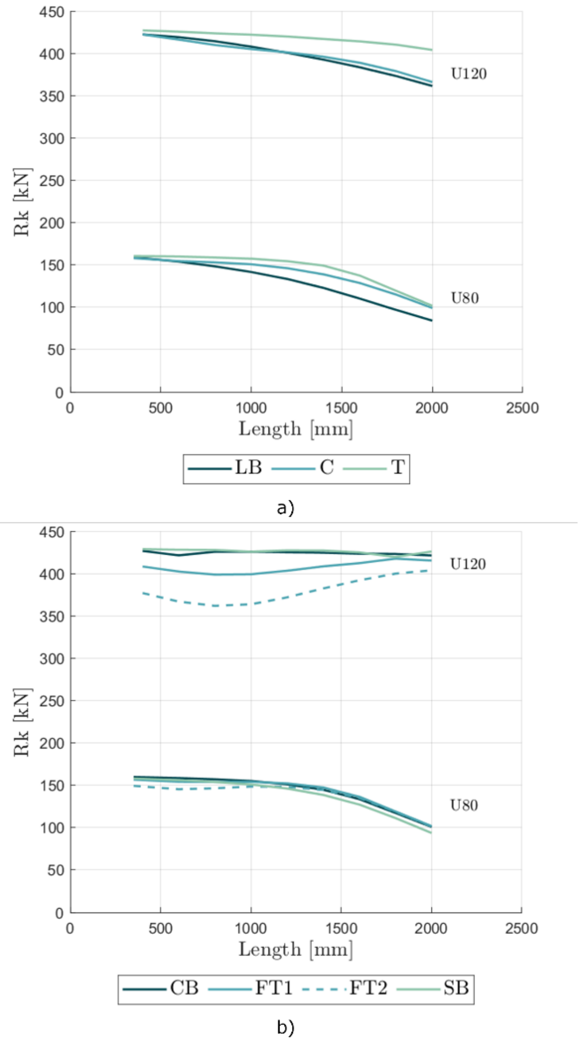

Figure 6 Influence of the geometric imperfections individually in the ultimate resistance of the upright. a) Global b) Local

It can therefore be concluded that the thickness of the upright plays a crucial role in determining the level to which geometric imperfections affect its performance. This is particularly evident in the case of local imperfections, where the transition from the U120 model, with a thickness of 3 mm, to the U80 model, with a thickness of 1.8 mm, results in a significant increase in their influence. For instance, in the case of springback, while its effect on the U120 upright is almost negligible, in the U80 model it leads to a reduction in buckling capacity of up to 38%.

After analysing the effect of each imperfection individually, simulations were performed with different combinations of imperfections to evaluate their interaction effects. A total of 48 different combinations were examined, with longitudinal bow considered in each one, as it was identified as the most critical imperfection and the most observed one in the experimental measurements. In every case, longitudinal bow was paired with one type of flare, chosen for its significance and variability. In the case of camber, three camber conditions were considered: none, positive, and negative. For the other imperfections, only two conditions were analysed: with and without the imperfection.

Figure 7 shows the most and least critical combinations for each upright at each length, which vary between cases. It can be observed that the effect of an imperfection combination can differ depending on the length of the section. The most notable cases are "LB + FT2 + CB" for the U120 upright and "LB + FT2 + CB + SB" for the U80. These combinations stand out due to their variability, as they are among the most influential in reducing the strength of short members, while having the least impact on longer ones.

In the case of the least critical combinations, these can increase the resistance of the uprights when compared to scenarios where only longitudinal bow is analysed, while the most critical combinations have a more significant negative effect.

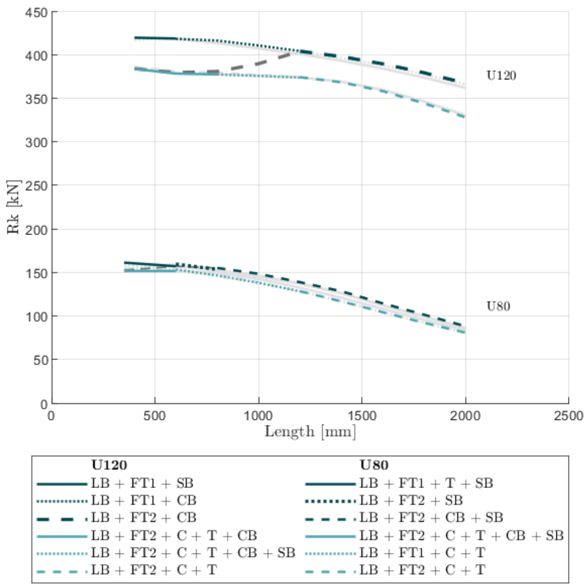

Figure 7 Influence of the combined geometric imperfections in the ultimate resistance of the upright.

7 Conclusions

This study presents a methodology for modelling the geometric imperfections that come from the roll forming process, in which these imperfections are measured, defined, and characterised. This tool has been validated with experimental data.

Based on this modelling, an analysis was conducted to detail the effect that each imperfection may have on the resistance of the upright. It was found that, primarily, global imperfections have the greatest impact, with longitudinal bow standing out among the others, followed by camber. Furthermore, the effect of a geometric imperfection on an upright varies depending on its geometry: the distance of the web, the flanges, and primarily its thickness.

It has also been observed that the effect of local imperfections on the uprights is more variable among different profiles, with significant variations depending on their geometry. As a result, these local imperfections remain highly unpredictable. Further investigation is therefore required to better understand the role they play in the resistance of the upright and their influence on its overall behaviour. Additionally, the effect of combinations of imperfections has proven to be relevant, as their interaction can notably influence the overall structural behaviour.

References

[1] Halmos, G. T. (2005) *Roll Forming Handbook.* CRC.

[2] Moneke, M; Groche, P. (2021) *The origin of end flare in roll formed profiles. International Journal of Material Forming*, 14(6), p. 1439–1461.

[3] Bonada, J; Casafont, M; Roure, F; Pastor, M. M. (2012) *Selection of the initial geometrical imperfection in nonlinear FE analysis of cold-formed steel rack columns. Thin-Walled Structures*, 51, p. 99–111.

[4] Sena Cardoso, F; Rasmussen, K. J. R. (2016) *Finite element (FE) modelling of storage rack frames. Journal of Constructional Steel Research*, 126, p. 1–14

[5] Bonada, J; Pastor, M. M; Roure, F; Casafont, M. (2015) *Influence of the cold work effects in perforated rack columns under pure compression load. Engineering Structures,* 97, p. 130–139.

[6] Xu, D; Wang, Y; Liu, X; Chen, B; Bu, Y. (2023) *A novel method and modelling technique for determining the initial geometric imperfection of steel members using 3D scanning. Structures*, 49, p. 855–874.

[7] E.N. 15512 (2020) *Steel static storage systems – Adjustable pallet racking systems – Principles for structural design.* Brussels. European Committee for Standardization (CEN).

[8] Pastor, M.M; Casafont, M; Bonada, J; Roure, F. *Imperfection amplitudes for nonlinear analysis of open thin-walled steel cross-sections used in rack column uprights. Thin-Walled Structures*, 76, p. 28–41.

[9] European Standard EN 1993-1-5:2006/AC:2009. (2009) *Eurocode 3 – design of steel structures – Part 1–5: Plated structural elements*. Brussels. European Committee for standardization (CEN).

Acknowledgements

The authors gratefully acknowledge the technical and material supply from AR-racking.